

RESEARCH

Open Access



Nanotechnology and cancer: improving real-time monitoring and staging of bladder cancer with multimodal mesoporous silica nanoparticles

Sean K Sweeney^{1,2}, Yi Luo³, Michael A O'Donnell⁴ and Jose Assouline^{1,2*}

*Correspondence:

jose-assouline@uiowa.edu

² NanoMedTriX, LLC, 2500

Crosspark Road, Suite E119,

Coralville, IA 52241-4710, USA

Full list of author information

is available at the end of the article

Abstract

Background: Despite being one of the most common cancers, bladder cancer is largely inefficiently and inaccurately staged and monitored. Current imaging methods detect cancer only when it has reached “visible” size and has significantly disrupted the structure of the organ. By that time, thousands of cells will have proliferated and perhaps metastasized. Repeated biopsies and scans are necessary to determine the effect of therapy on cancer growth. In this report, we describe a novel approach based on multimodal nanoparticle contrast agent technology and its application to a preclinical animal model of bladder cancer. The innovation relies on the engineering core of mesoporous silica with specific scanning contrast properties and surface modification that include fluorescence and magnetic resonance imaging (MRI) contrast. The overall dimensions of the nano-device are preset at 80–180 nm, depending on composition with a pore size of 2 nm.

Methods: To facilitate and expedite discoveries, we combined a well-known model of bladder cancer and our novel technology. We exposed nanoparticles to MB49 murine bladder cancer cells *in vitro* and found that 70 % of the cells were labeled by nanoparticles as measured by flow cytometry. The *in vivo* mouse model for bladder cancer is particularly well suited for T1- and T2-weighted MRI.

Results: Under our experimental conditions, we demonstrate that the nanoparticles considerably improve tumor definition in terms of volumetric, intensity and structural characteristics. Important bladder tumor parameters can be ascertained, non-invasively, repetitively, and with great accuracy. Furthermore, since the particles are not biodegradable, repetitive injection is not required. This feature allows follow-up diagnostic evaluations during cancer treatment. Changes in MRI signals show that *in situ* uptake of free particles has predilection to tumor cells relative to normal bladder epithelium. The particle distribution within the tumors was corroborated by fluorescent microscopy of sections of excised bladders. In addition, MRI imaging revealed fibrous finger-like projections into the tumors where particles insinuated themselves deeply. This morphological characteristic was confirmed by fluorescence microscopy.

Conclusions: These findings may present new options for therapeutic intervention. Ultimately, the combination of real-time and repeated MRI evaluation of the tumors

enhanced by nanoparticle contrast may have the potential for translation into human clinical studies for tumor staging, therapeutic monitoring, and drug delivery.

Keywords: Mesoporous silica nanoparticles, Transitional cell carcinoma, Bladder, Magnetic resonance imaging, Cystoscopy, Mouse orthotopic tumor model

Background

Transitional Cell Carcinoma (TCC) of the bladder is the fifth most common malignancy in the United States (Siegel et al. 2015). Although the majority of human bladder cancer is superficial at the time of detection, the recurrence rate and the risk of progression to advanced disease are high (Hall et al. 2007; Kaufman et al. 2009; Faba et al. 2012; Nargund et al. 2012). Currently, the most common screening method is cystoscopy (Liu et al. 2012), which includes white light as well as fluorescent or narrow band cystoscopy (Kriegmair et al. 1994; Filbeck et al. 2002; Joudi and Konety 2004). The fluorescent and narrow band methods aim to highlight or differentiate the tumor from normal bladder epithelium wall using broad range/non-specific fluorescent dyes or stains (Filbeck et al. 2002; Joudi and Konety 2004). These generic labeling methods are not aimed at any particular molecule, but rather colorize the entire bladder with the hope that some differential labeling may occur. Macroscopic tumors can be seen with these methods, but smaller lesions may be missed (Zaak et al. 2005; Grossman et al. 2006). In addition, suspicious smaller lesions need biopsy for cancer staging, as cystoscopy alone remains insufficient (Cheng et al. 2000, 2009; Mitra et al. 2012).

The development of diagnostic tools for TCC has been slowed by the lack of an optimal animal model for the disease, due to the anatomical inaccessibility and the relative lack of molecular and bioinformatics data on the genetic diversity of the specific tumors. A variety of experimental models have been tested with mixed success, including mice (Chan et al. 2009; Zhang et al. 2015), rabbits (Nemoto et al. 1981), and primates (Cozzi et al. 2001). The current standard is a mouse orthotopic tumor model in which a known TCC cell line (MB49) is implanted following chemical disruption of the normal epithelium (Soloway et al. 1973; Bockholt et al. 2012; Newton et al. 2014). This cell line has similar features and replicates the pathobiology of human homologues (Luo et al. 2004). Although the presence of reporter genes has allowed for some measurements of non-invasive real-time tumor growth, no methods have been described capable of providing 3-dimensional details of growth, including heterogeneities within the tumor, in real time.

In addition to diagnostic tools, therapeutic options for TCC are limited by anatomical challenges. After initial resection, many patients undergo bacillus Calmette-Guerin (BCG) immunotherapy; however, the recurrence rate for BCG is up to 50 % (Hall et al. 2007; Faba et al. 2012). Furthermore, many patients cannot complete the therapy due to the risks of sepsis and other side effects (Lamm et al. 2000; Brausi et al. 2014). Thus, groups have attempted to package an attenuated form of the BCG cell wall skeleton into nanoparticles to more safely induce an immune response, with mixed results (Ochiai et al. 1983; Nakamura et al. 2014). Many other forms of nanoparticles are used as carriers of chemotherapeutics; (Connolly et al. 2012; Huang et al. 2012) these, however, often cannot be visualized/detected and have poor retention in the bladder. Very few examples exist of chemical agents that can be used both for detection and therapeutic solutions.

For example, radioactive agents produce quality PET/SPECT images, (Hoiland-Carlsen et al. 2014; Bouchelouche and Choyke 2015) but have short half-lives, necessitating repeated doses for longitudinal studies, further increasing the patients' exposure to ionizing radiation. Thus, there is a need for an advanced compound which would provide a good image using lowered-cost equipment (ultrasound, MRI), with no ionizing radiation and with good retention in the bladder for follow-up growth evaluation. The development of a single agent capable of providing sequentially valuable information from MRI as well as ultrasound contrast [image-guided surgical techniques (Nyland et al. 2002; Gkritsios et al. 2014)] would be highly desirable.

Mesoporous silica nanoparticles (MSNs) are often studied as vehicles for drug delivery due to their large ratios of pore volume and surface area to weight relative to other nanomaterials (Giri et al. 2005; Gruenhagen et al. 2005; Slowing et al. 2007; Chen et al. 2010; Benezra et al. 2011). Once injected, MSNs are bioinert, non-toxic and well-tolerated at clinically relevant concentrations (Slowing et al. 2006; Lu et al. 2008, 2010), unlike biodegradable polymers that can generate toxic byproducts (Athanasίου et al. 1996; Semete et al. 2010), or nanomaterials with reactive elements such as quantum dots (Kirchner et al. 2005; Liu et al. 2014). In addition, the use of MSNs in imaging applications is an area of active research. In particular, MSN are used to label and track cells through functionalization with fluorophores (Giri et al. 2005; Chen et al. 2010; Benezra et al. 2011), paramagnetic materials for magnetic resonance imaging (MRI) (Chen et al. 2010; Hsiao et al. 2008; Larsen et al. 2009), or electron dense materials for computed tomography (CT) (Chen et al. 2010; Luo et al. 2011).

Here, we describe the application of a novel MSN tool for noninvasive and longitudinal tracking of bladder cancer, using an established *in vivo* mouse model for the disease. Murine bladder cancer cells (MB49) were found to take up the MSN *in vitro*; in the mouse bladder, the MSN were taken up preferentially by tumor cells more readily than healthy bladder epithelium. The MSN were further functionalized with a peptide found to bind specifically to bladder cancer cells, thus improving specificity. The MSN facilitated the use of tumor imaging/staging *in vivo* using MRI, and *ex vivo* using fluorescent microscopy. This study presents the potential of these MSN to improve tumor visualization and staging, thereby improving patient outcomes.

Methods

Reagents

Gadolinium (III) chloride hexahydrate ($\text{GdCl}_3 \cdot 6\text{H}_2\text{O}$), cetyltrimethylammonium bromide (CTAB, $\text{CH}_3(\text{CH}_2)_{15}\text{N}(\text{CH}_3)_3\text{Br}$), diethylene glycol, tetraethoxysilane (TEOS), and (3-aminopropyl)trimethoxysilane (APTMS) were purchased from Alfa Aesar (Ward Hill, MA). Sodium hydroxide (NaOH) was purchased from VWR (Radnor, PA). Methanol, dimethyl sulfoxide (DMSO), and toluene were purchased from Fisher Scientific (Pittsburgh, PA). Tetramethylrhodamine isothiocyanate (TRITC) was purchased from Sigma-Aldrich (St. Louis, MO). 2-[Methoxy(polyethyleneoxy)propyl]trimethoxysilane was purchased from Gelest (Morrisville, PA). Dulbecco's modified eagle medium (DMEM), Roswell Park Memorial Institute (RPMI) 1640 medium, fetal bovine serum (FBS), and penicillin–streptomycin (pen-strep) were purchased from Life Technologies (Grand Island, NY).

Particle synthesis/characterization

First, a gadolinium oxide colloid was obtained following the previously reported synthesis (Bridot et al. 2007): $\text{GdCl}_3 \cdot 6\text{H}_2\text{O}$ (11.53 g) was dissolved in 200 mL of diethylene glycol at 60 °C overnight under vigorous stirring. Aqueous NaOH (7.5 mL, 3 M) was added and the solution was heated at 140 °C for 1 h and then at 180 °C for 4 h. The obtained transparent colloid of gadolinium oxide nanoparticles was stored at room temperature. CTAB (1.0 g, 2.745 mmol) was dissolved in nanopure water (480 g, 26.67 mol), followed by the addition of NaOH solution (2.0 M, 3.5 mL, 7.0 mmol). The mixture was heated to 80 °C for 1 h. To this clear solution, TEOS (4.7 g, 22.56 mmol) was added drop wise, followed by immediate addition of 1 mL of the gadolinium oxide colloid. The reaction was stirred vigorously at 80 °C for 2 h, then the CTAB surfactant was removed by Soxhlet extraction with methanol for 24 h and then dried under vacuum to obtain gadolinium oxide functionalized mesoporous silica nanoparticles ($\text{Gd}_2\text{O}_3\text{-MSN}$). Next, TRITC (5.7 mg, 0.0128 mmol) was reacted with APTMS (2.2345 μL , 0.0128 mmol) in DMSO for 2 h, and TRITC- $\text{Gd}_2\text{O}_3\text{-MSN}$ was prepared by grafting 0.05 mL of the resulting product on the previously synthesized $\text{Gd}_2\text{O}_3\text{-MSN}$ (100 mg) in toluene under reflux for 24 h. The resulting solution was filtered and the obtained pink solid was washed with copious amount of methanol and then dried under vacuum. Finally, the particles were further functionalized with poly(ethylene glycol) (PEG) by grafting 2-[Methoxy(polyethyleneoxy)propyl] trimethoxysilane (0.2 mmol) on TRITC- $\text{Gd}_2\text{O}_3\text{-MSN}$ (100 mg) in toluene under reflux for 24 h. The resulting solution was filtered and the obtained pink solid (PEG-TRITC- $\text{Gd}_2\text{O}_3\text{-MSN}$) was washed with copious amount of methanol and then dried under vacuum.

The materials were characterized by X-ray diffraction, using a Rigaku Ultima IV diffractometer, nitrogen sorption analysis in a Micromeritics ASAP 2020 surface area and porosity analyzer using the Brunauer-Emmett-Teller equation to calculate surface area and pore volume and the Barrett-Joyner-Halenda equation to calculate the pore size distribution. Dynamic light scattering (DLS) was used to obtain particle size distribution and zeta potential data, using the Malvern Zetasizer Nano ZS instrument. The materials were also visualized by transmission electron microscopy (TEM) by supporting samples on copper grids in a Tecnai G2 F20 microscope operating at 200 kV.

Cell culture/labeling

Murine TCC cell line MB49 (Summerhayes and Franks 1979) and human TCC cell line T24 (Bubenik et al. 1973) are well-established; here, MB49 cells transfected with either green fluorescent protein (GFP) or luciferase (luc) reporter genes, and normal T24 cells were cultured in RPMI 1640 medium supplemented with 10 % FBS and pen-strep. Cells near confluence on tissue culture plastic were exposed to PEG-TRITC- $\text{Gd}_2\text{O}_3\text{-MSN}$ at a concentration of 100 $\mu\text{g}/\text{mL}$ for 16 h. Flow cytometry was used to measure the proportion of labeled MB49-GFP⁺ cells, while fluorescent microscopy was used to evaluate labeling on T24 cells. Prior to in vivo experiments, labeled and non-labeled cells were counted and the viability measured using trypan blue exclusion dye.

In vivo tumor implantation

All procedures were performed according to NIH guidelines and previously approved by the Institutional Animal Care and Use Committee (IACUC). Intravesicular instillation of

tumor cells was performed according to previously described methods (Luo et al. 2004). Female C57Bl/6 mice were anesthetized with a ketamine/xylazine mixture. The bladder was chemically burned by instillation of 5 μ L 0.2 M silver nitrate, followed by rinsing with 100 μ L phosphate buffered saline (PBS). A 50 μ L suspension containing 5×10^5 MB49-Luc⁺ cells in 50 % normal mouse serum was instilled into the bladder and retained for 1 h by catheter exclusion. Additional boluses of 1×10^5 tumor cells were injected subcutaneously in the left and right flank. In initial experiments designed to determine maximum signal, cells were labeled with MSN prior to instillation; in later studies designed to be more clinically relevant, the tumor was established prior to instillation of free MSN particles (1 mg MSN/50 μ L PBS). Negative control mice were instilled with sham (saline) injections, followed by instillation of free MSN following the same timing as tumor mice.

Imaging/image processing

Images were acquired 24 h after instillation of particles to allow for the elimination of free particles through urination. *From 1–8 days following tumor implantation*, in vivo fluorescence and luminescence were measured using the IVIS 200 with appropriate settings for detection of GFP, TRITC, and luciferase activity following intraperitoneal injection of 1.5 mg luciferin. MRI scans were acquired using the Unity/INOVA 4.7 T small animal scanner (Varian, Palo Alto, CA) with a 25-mm gradient RF coil and fast spin echo multislice (fsems) sequences with T1- or T2-weighting (T1-weighted scans: $T_R = 800$ ms, $T_E = 15$ ms, echo train length = 8, number of averages = 10; T2-weighted scans: $T_R = 2000$ ms, $T_E = 15$ ms, echo train length = 8, number of averages = 10). Typical image dimensions are 512×512 with 30 slices and a voxel size of $0.068 \times 0.068 \times 0.4$ mm. Scans were saved as DICOM image stacks, which were converted to NIFTI format and preprocessed using a MATLAB routine developed in the lab, following a method of background removal Salvado et al. (2006a, b) and interpolation by reverse diffusion Salvado et al. (2006a, b). Using the free medical image processing software MIPAV, scans were normalized to one another by assigning a value of 1000 to the average intensity of fat adjacent to the kidneys, with all other values linearly interpolated between 0 and 1000. Volumes of interest (VOIs) were either manually drawn or semi-automatically selected using the “levelset VOI” tool in MIPAV.

Histopathology and statistical analyses

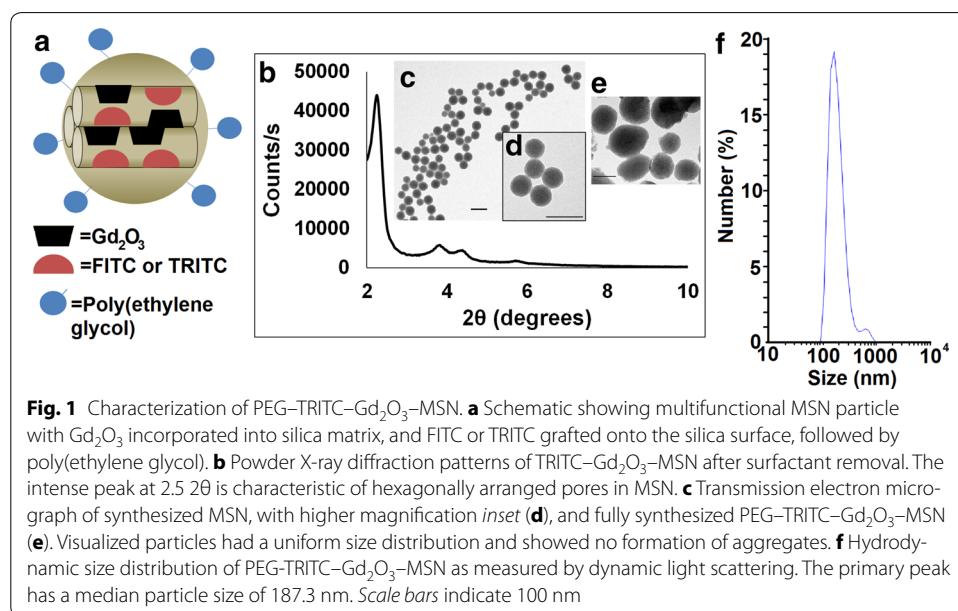
Following the MRI scans, mice were euthanized by CO₂ inhalation. The bladders were excised, embedded in OCT medium, flash frozen in liquid nitrogen and sectioned. A portion of the sections were mounted on glass slides without stain for use in fluorescence microscopy, while adjacent sections were stained with hematoxylin and eosin for histological analysis. Fluorescence images were acquired using standardized camera settings (Olympus DP70 camera, 1360×1024 resolution, and 15 s exposure time), while corresponding bright field images were acquired using the same resolution and the camera's auto-exposure setting with color correction. The average red fluorescence intensity of each 10 \times field was quantified by isolating the red channel and using VOI tools to isolate regions of tissue from the background, using the bright field images as a reference for identifying the tissue and background. The average fluorescence intensity of each image was normalized by dividing it by the average intensity of the background. Comparisons of

measurements between groups of mice were made using Student's unpaired *T* test with an alpha level of 0.05 considered significant. Comparisons of different tumors within the same mouse were made using a two one-sided *t*-test (TOST) (Hong et al. 2015) with a significance level of $\alpha = 0.05$ and a test margin of 0.05 (a unitless value of normalized MRI intensity), representing the average smallest difference between two intensities that our image processing technicians could discern with the naked eye.

Results and discussion

Particle characterization

We synthesized multifunctional MSN for in vivo imaging of bladder tumors according to the schematic (Fig. 1a). By incorporating Gd_2O_3 into the silica matrix and covalently grafting FITC or TRITC onto the particle surface, the MSN is functionalized for fluorescent and MRI imaging modalities. Systematic characterization was performed at each step in the process of synthesizing the PEG-TRITC- Gd_2O_3 -MSN. Powder XRD analysis confirmed hexagonally arranged mesopores in the diffraction pattern of the Gd_2O_3 -MSN as evident by the intense d_{100} , and well resolved d_{110} and d_{200} peaks characteristic for MSN (Fig. 1b). Transmission electron micrographs of the Gd_2O_3 -MSN particles showed this pattern as well as uniform size distributions and good dispersibility with little aggregation (Fig. 1c-e, inset). Nitrogen sorption analysis of the TRITC- Gd_2O_3 -MSN exhibited a Type-IV isotherm, typical of mesoporous materials, with a BET surface area of $710 \text{ m}^2\text{g}^{-1}$. The average pore diameter for TRITC- Gd_2O_3 -MSN by BJH calculation is 24 \AA . The fully synthesized PEG-TRITC- Gd_2O_3 -MSN was characterized by DLS; the median hydrodynamic diameter of the particles was 187.3 nm , with 96.3% of the particles falling within the primary distribution peak, spanning between 90 and 400 nm , resulting in a polydispersity index (PDI) of 0.535 (Fig. 1f). The number of particles greater than 400 nm (likely aggregated MSN) is less than 4% of the total and does not have adverse experimental implications on the tagging of bladder tumors. Prior to use



in tissue culture or in vivo, the fluorescence (FITC or TRITC) was measured using serial dilutions in a fluorimetric plate reader. In order to eliminate unbound fluorophores from the suspension, the particle suspensions were repeatedly rinsed in phosphate buffered saline and centrifuged until no detectable fluorescence was observed in the supernatant.

Labeling/flow cytometry

Particle uptake by TCC cells was determined by flow cytometry. GFP⁻/TRITC⁻ cells were used to establish the threshold for detection (Fig. 2a) while the GFP⁺/TRITC⁻ cells were used to confirm the efficiency of GFP transfection, which was found to be 99.8 % (Fig. 2b). In the final sample, 69.6 % of the cells were found to be GFP⁺/TRITC⁺ (Fig. 2c), with a wide range of levels of rhodamine fluorescence, indicating some cells picked up more MSN particles than others.

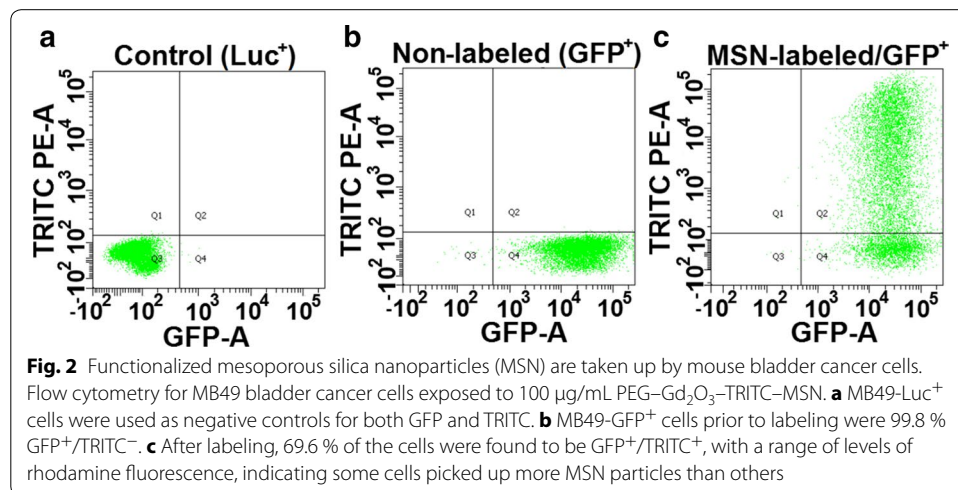
In vivo fluorescence

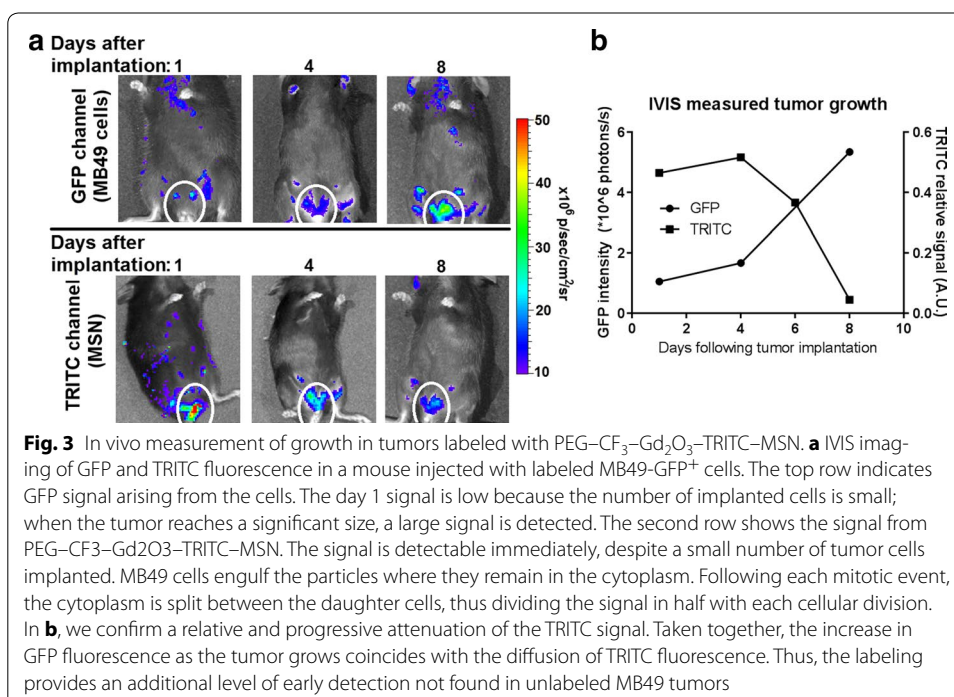
Implantation of PEG–TRITC–Gd₂O₃–MSN-labeled MB49-Luc⁺ and MB49-GFP⁺ cells was confirmed using in vivo luminescence and fluorescence (Fig. 3). Using the standard detection methods (luciferin luminescence or GFP fluorescence), the tumor was detectable within 6–8 days in vivo, consistent with previous results. Using the MSN for detection (TRITC fluorescence), the tumors were detectable in 1–4 days (Fig. 3b). The growth rate was consistent with that of unlabeled tumor cells, indicating that the particles are not inhibitive of tumor growth.

MRI imaging

We implemented two tumor labeling approaches, representing incremental stages moving towards translational significance. In the first, we labeled cells prior to implantation to determine the maximal MRI signal attainable. Subsequently, we implanted the tumor cells first, labeling them in vivo, to represent a clinically relevant scenario.

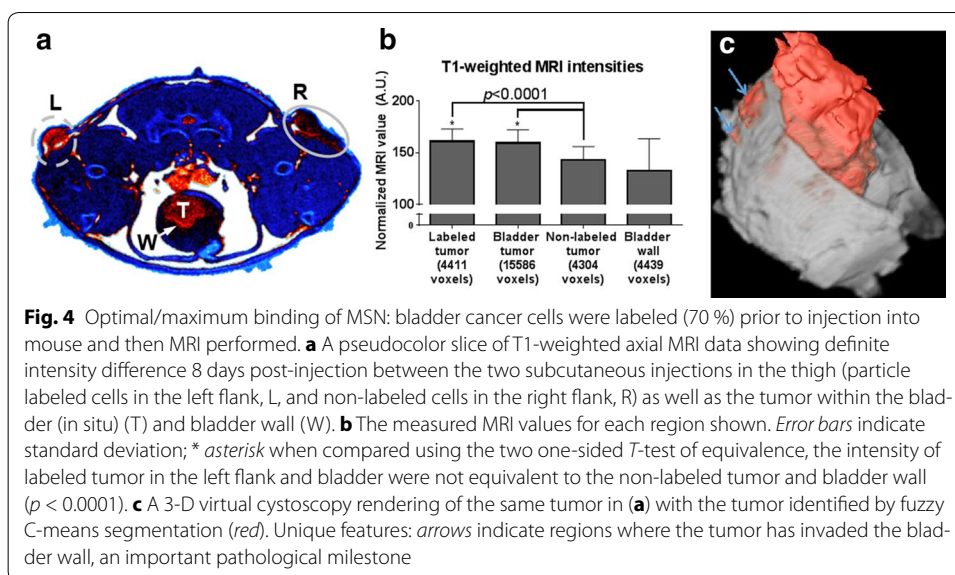
1. To determine the maximum MRI signal, MB49-Luc⁺ cells were labeled with PEG–Gd₂O₃–TRITC–MSN prior to instillation in the bladder to obtain the best possible contrast in MRI. Tumors were also implanted in the left and right flank, using labeled and non-labeled cells, respectively, as controls. With T1-weighting, a hyperinten-





sity was observed for tumors comprised labeled cells relative to non-labeled cells (Fig. 4a). After segmentation, the normalized MRI values of labeled (161.2 ± 11.8) versus non-labeled (143.3 ± 12.9) flank tumors were compared using the TOST test for equivalency with a test margin of 0.05 and found to be non-equivalent at a significant ($p < 0.0001$) level (Fig. 4b). Further, the tumor instilled into the bladder (159.5 ± 12.8), also comprised MSN-labeled cells, was found to be equivalent to the flank tumor comprised labeled cells ($p > 0.05$) and non-equivalent to the tumor comprised non-labeled cells ($p < 0.001$). This initial test also confirmed that the process of labeling MB49 cells with MSN did not alter their ability to engraft, either subcutaneously or in the bladder. Three-dimensional rendering of the tumor shows infiltration of the bladder wall, potentially metastasizing to nearby tissues (Fig. 4c). This represents clinically important data for tumor staging.

- To represent a more clinically relevant scenario, we subsequently injected MB49 tumors to establish the tumor, then after 8 days we labeled in vivo via intravesicular instillation of colloidal PEG-Gd₂O₃-TRITC-MSN particles (1 mg MSN in 50 μ L PBS). MRI scans showed immediately before and 1 day after MSN addition to determine the qualitative effects of the MSN on tumor characterization as well as the quantitative changes in T1- and T2-weighted MRI signal for bladder tumor relative to normal bladder epithelium. A representative 2-D slice of T2-weighted MRI of the same tumor is shown before (Fig. 5a) and 24 h after (Fig. 5d) addition of MSN particles. Each pair of images is shown after normalization, using equivalent input-output color maps. Additional 3-D renderings of the tumor in situ (Fig. 5b, e) and segmented (Fig. 5c, f) reveal unique features within the tumor, including finger-like projections which have a different consistency than the bulk of the tumor and can be traced along the outer boundary. Quantitatively, the animals with tumors showed a



much larger magnitude of change in normalized MRI value after administration of particles than the bladder walls of non-tumor, sham-injected negative control mice (Fig. 6). This result provides evidence that in vivo tumors take up MSN particles with a higher affinity than normal bladder epithelium. The projections were found to be considerably hypointense in these renderings of T2-weighted scans, indicative that in larger tumors, a subset of cells have an especially high affinity for the MSN.

Histological analyses

To validate and confirm MRI observations, we process tissues for histological evaluation. The bladders were excised after the final MRI scans, re-scanned for whole tissue fluorescence signal using the IVIS system, and then serially sectioned. Gross anatomical observations using IVIS show, as expected, only the Luc⁺ tumor showing luciferase luminescence, while both the GFP⁺ and Luc⁺ tumor have positive fluorescence in the red channel, indicating retention of the PEG–Gd₂O₃–TRITC–MSN (Fig. 7). The finger-like projections seen in MRI (Fig. 5f) were observed to be regions of higher cell density/faster growth (Fig. 5g), and are consistent with observations made of TCC in humans (Cheng et al. 2009). Additionally, the fluorescence micrograph (Fig. 5h) corroborates the MRI scan, showing that these are the areas of greatest particle uptake. In both the T1- and T2-weighted MRI scans, we observed clear improvements in boundary delineation. This allowed for the in vivo evaluation of features such as the bladder wall with a level of detail approaching that of histological sections (Fig. 8). Based on measurements collected from both MRI and histological sections, we calculated the thickness of the bladder wall to be approximately 1.00 mm, corresponding to 17 pixels at our achievable resolution.

This report documents the findings on an orthogonal mouse model, and the potential for translation to clinical use of a novel nanoparticle-based technology. This approach may improve diagnostic and potentially therapeutic outcomes in TCC of the bladder. We are unaware of clinically relevant gold standards to use for a comparative basis. Clinical

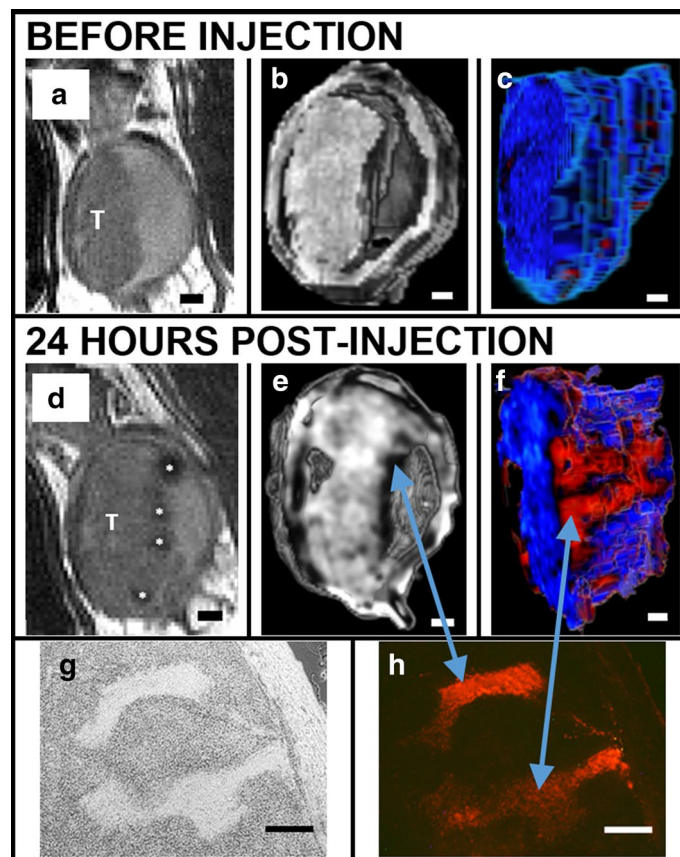


Fig. 5 Evaluation of increased contrast and histopathological benefits of our nanoparticle technology. MSN bind preferentially to bladder cancer cells relative to normal bladder epithelia in vivo as shown in a series of renderings of T₂-weighted MRI scans acquired before (**a–c**) and after (**d–f**) intravesicular instillation of Gd₂O₃-TRITC-MSN. **a** and **d** 2-dimensional grayscale view, the tumor (T) is shown before and after injection of particles; note clear labeling of the tumor surface * *asterisk*. (**b, e**) 3-dimensional rendering provides further evidence of the particle distribution on the tumor surface. **c, f** Here the tumor is segmented and rendered with a pseudocolor map. Finger-like projections are revealed which are not observed before the injection of particles (**c**). Histology confirms anatomical observations and particle penetrations in the structures within the tumor: *bright field* (**g**) and fluorescent microscopy (**h**). Scale bars 1 mm (**a–f**); 250 μm (**g, h**)

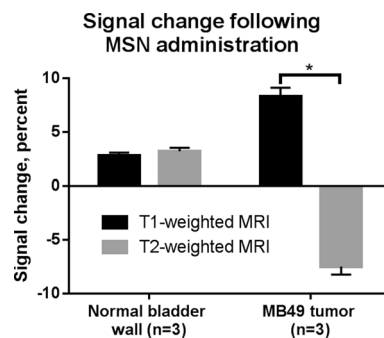
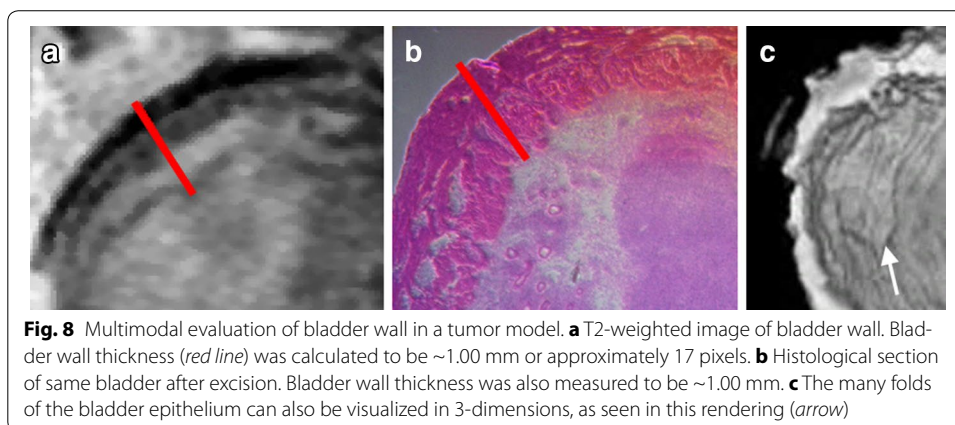
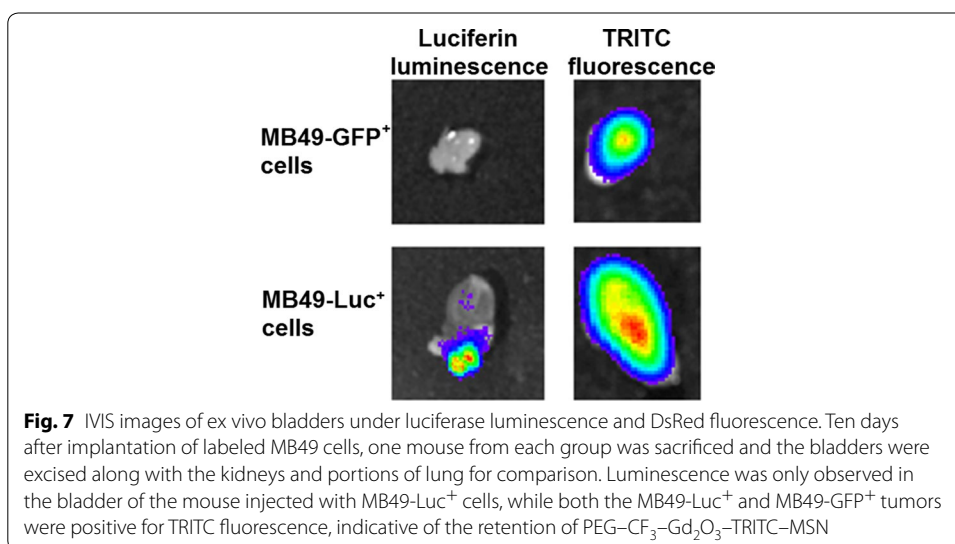


Fig. 6 T₁ and T₂ signal changes specific to the in vivo bladder tumor as the result of particle injections. The normalized average MRI intensities of bladder tumor and normal (sham-injected, negative control) bladder wall were measured before and after administration of MSN. The result was an increase in apparent T₁ intensity and a decrease in T₂ intensity in tumor bladders, compared with minimal change in the normal bladder wall (*-*p* < 0.0001)



approaches include ImmunoCyt/uCyt[™], a fluorescent test that uses three monoclonal antibodies (Vergara-Lluri et al. 2014), and UroVysion[™], which is an in situ hybridization test using four different probes to different chromosomes (Seideman et al. 2015). We are aware of the benefits of Hexvix, or hexyl aminolevulinate, which is similar to a chemical found naturally in the body and contains porphyrins (Martoccia et al. 2014). The underlying principle of this approach is that cancer cells absorb this substance faster than healthy cells and turn fluorescent pink when the cystoscope light changes from white to blue. To date, we have not seen a report of cystoscopy-based approaches used in murine models.

Using the well-established MB49 murine line of bladder cancer cells, the uptake of our particles was measured in vitro, followed by non-invasive detection of labeled, implanted tumors in vivo using magnetic resonance imaging. In a pre-clinical animal model for bladder cancer, free particles were instilled in bladders with pre-established tumors. We demonstrate that the localization of the particles highlighted to the tumor helped delineate its edges and other features which were not otherwise detectable. We identified finger-like projections-areas which are consistent with the literature and are believed to be

connective cellularized tissue (Cheng et al. 2000). These tumor penetrating structures displayed a higher particle uptake than the surrounding tumor. It is tempting to envision the potential therapeutic applications of the particles as they are able to access the inner cellular components of the tumor.

Two major hindrances to the recovery and poor prognostics of this form of cancer is the delay in detection of the cancer and its subsequent propensity to rapidly metastasize to adjacent tissue (Faba et al. 2012; Kaufman 2006). Although TCC is among the most deadly forms of cancer, the methods for diagnosis, including fluorescent and colored dyes that “paint” the bladder wall and delineate the tumor for use with cystoscopic techniques, however, are lacking in both depth of penetration and accuracy (Liu et al. 2012; Bryan et al. 2014). Because the depth of tumor penetration is difficult to grade through cystoscopic means alone, the bladder is often removed as a precautionary measure, to the severe detriment of quality of life for the patient (Kaufman et al. 2009; Dalbagni et al. 2009; Gakis et al. 2013). Our results show a novel option based on a core of MSN for multimodal use in cancer diagnostics. In addition, the potential is clear for the material to be used therapeutically, as a carrier of anti-tumor agents. The engineered nanoparticles are made to improve visualization of the tumor through T1- and T2-weighted computational MRI techniques.

Using the well-established MB49 murine TCC line in culture, we found 69.6 % of cells to be labeled with our PEG-Gd₂O₃-TRITC-MSN, with most cells fluorescing between 2 and 3 orders of magnitude above the detection threshold for the flow cytometry instrument. The particles were well tolerated by the cells; viability of labeled cells remained high (over 90 %) as indicated by trypan blue exclusion dye measurement and by virtue of the successful engraftment of labeled tumor cells *in vivo*. The manner of uptake has not yet been characterized, though from the literature and our own observation it is most likely that particles are engulfed by phagocytosis. The uptake mechanism of similarly sized and functionalized MSN has been characterized by other groups as co-localized with endosomes (Slowing et al. 2006; Hsiao et al. 2008). These studies have examined the involvement of clathrin-coated pits, using inhibition of clathrin to show reduced uptake (Huang et al. 2005), and lysosomes, using fluorescent lysosomal tracking dyes (Slowing et al. 2006). Additional determination of uptake awaits future experimentation with specific cell signaling molecules on the MSN surface.

The current standard pre-clinical model for TCC is the mouse orthotopic model in which MB49 murine TCC cells are implanted onto a chemically disrupted bladder epithelium (Luo et al. 2004). Although the model presents a number of advantages, i.e., it reliably creates tumors which closely mirror the histological picture of human TCC, we found that the tumor growth varies greatly depending on the quality of the chemical disruption and the number of cells that bind to it. In addition, the small size of this animal model does not lend itself to cystoscopy or other clinically relevant screening techniques. In this report, we show that by combining the animal model with the image improvement offered by our MSN, we can use small animals (mice) and create valuable virtual cystoscopy. Our early experiments involved labeling of cells with our particles prior to implantation in order to optimize our imaging parameters, and to show that labeled cells will engraft and grow in a similar manner to non-labeled tumor cells. Control injections of labeled and non-labeled cells implanted subcutaneously in either

thigh of the mouse showed similar growth characteristics, indicating that cell labeling alone did not adversely affect tumor growth or implantation. Importantly, our technology allows for the non-invasive detection of histological features. Within the bladder, the tumor boundary was more easily delineated, and was observed to cross the bladder wall. These crucial data regarding depth of tumor penetration are impossible to obtain clinically through cystoscopy alone (Cheng et al. 2000, 2009; Mitra et al. 2012).

Our experimentation strategy was first to establish a bladder tumor model in which nanoparticles would be most visible and then refine our approach to develop a method with more clinical relevance where the tumor was initiated in the bladder, then followed by injection and binding in vivo of free MSN 8 days later. Interestingly, prior to the instillation of particles, the MRI scan shows a very homogeneous tumor which reflects the uniformity of the MB49 cells in culture. Only after administration of particles are unique heterogeneities revealed, which are correlated histologically. This includes the formation of finger-like projections, forming largely around the boundaries of the bulk tumor. These regions appear to be more fibroblastic in morphology, with a denser matrix of connective tissue than the bulk tumor, as evidenced by the higher relative amount of eosin staining. Furthermore, these regions have a higher affinity for our MSN than the bulk tumor; this is consistent with our observations, and those of other groups, (Hsiao et al. 2008; Selvan et al. 2010) that MSN are readily engulfed by fibroblast cells. To the best of our knowledge, nothing is published regarding the heterogeneity of MB49 tumors in situ, though groups have reported the presence of finger-like projections in human clinical pathological specimens. (Cheng et al. 2000).

The typical clinical tool for bladder cancer diagnosis is white light or fluorescent cystoscopy, used in conjunction with a form of dye that improves definition of the tumor boundaries (Kriegmair et al. 1994; Filbeck et al. 2002; Joudi and Konety 2004). Clinically, MRI virtual cystoscopy of the bladder is less commonly used, (Raza and Jhaveri 2012) and although gadolinium-based contrast agents are sometimes administered intravenously prior to scanning, specific agents that bind tumors are not yet available. Our results indicate that intravesicular instillation of MSN particles improves differentiation of the tumor in MRI; the signal obtained from normal bladder wall is unaffected by particle instillation, whereas the signal of the tumor increases under T1-weighted MRI, and decreases under T2-weighted MRI (Fig. 6). This is consistent with the accumulation of gadolinium-based contrast agents in tumors, and corroborated by the difference observed in fluorescence signals from excised bladders of tumor and normal mice (Fig. 5). In normal bladder epithelia, the particles that were retained appeared to be discretized in macrophages, whereas the tumor tissue possessed a brighter, more widespread fluorescence throughout, or in the case of more heterogeneous tumors, spread among a particular subpopulation of the tumor.

In this study, taking into account the consideration that clinical efficacy of using nanoparticles may be hindered or diminished due to bladder epithelium becoming hyper-permeable in TCC bladders (Brown et al. 1993; Gontero et al. 2004). The immediate implications being that particles may bind to non-tumor regions in a cancerous bladder, thus leading to overestimation of the true tumor size. We showed that has not been the case in our study, as we clearly demonstrate that our particles have a predilection for

cancerous tissue. Further improvement will have to wait for the development of specific targeting strategies.

With respect to image quality improvement, our current small animal scanner has a magnetic field of 4.7 T and is capable of in-plane image resolutions below 100 μm . At this resolution, we detected patterns in MRI corresponding to layers observed in histological sections, and visualized folding patterns within the bladder 3-dimensionally (Fig. 8). With the advent of MRI systems with magnets as large as 7 T and more powerful gradient coils, both in small animal and clinical use, we anticipate an improvement in signal/contrast for the same MSN formulation.

Thus, there is a need to improve with higher-specificity molecules. In addition to advances in imaging technology, the obtained signal can be further improved by increasing the specificity of the particles for bladder cancer cells. The particles presented thus far have not been functionalized for cell specificity; the specificity we observe is a result of exploiting the morphological differences between normal and tumor cells in the bladder. Whereas healthy/intact epithelium is defined by tight gap junctions and cell adhesion molecules only at the basement membrane, diseased (cancerous/inflamed) epithelium divides rapidly, has looser gap junctions, and overexpresses adhesion molecules, such as EpCAM (Bryan et al. 2014; Kowalski et al. 2010) integrins, (Knowles et al. 2013) laminin, cadherins, (Gontero et al. 2004) and other surface molecules (Parker et al. 2005; Tagaya et al. 2014). Due to these features, diseased epithelium has a higher affinity for foreign objects than normal epithelia. To improve upon this, our colleagues have identified a short peptide sequence using a phage display library with a high affinity for a wide range of bladder cancer cells across multiple species including mouse, dog, and human, and with little affinity for normal bladder epithelia. We intend to enhance the specificity of our particles through their functionalization with this peptide. To that end, we have developed a new particle capable of binding proteins/peptides through coupling chemistry (Hermanson 2008).

An additional desirable property of MSN particles which was not directly addressed in this study would be to have uptake and delivery of soluble materials within their porous structure. Many have successfully demonstrated delivery of bioactive agents in vitro using MSN (Giri et al. 2005; Gruenhagen et al. 2005; Slowing et al. 2007; Chen et al. 2010). The increased complexity of delivery in vivo makes it a more challenging scenario (Chan and Lin 2015; Wang et al. 2015). However, if some of these challenges can be overcome in the harsh chemical environment of the bladder, cancer treatment can be vastly improved. Whereas most chemotherapeutics are quickly eliminated from the bladder via urination (Grabnar et al. 2006; GuhaSarkar and Banerjee 2010), particles loaded with chemotherapeutics and retained by tumor cells will remain in the bladder for a longer time. Similarly, BCG immunotherapy can be improved through longer retention times, thus improving the depth of drug delivery, rather than simply removing the outermost cells a few layers at a time as current therapies tend to do (Kaufman 2006; Kim and Steinberg 2001).

Conclusions

This study represents a unique example of the synergistic use of MRI, nanoparticles and computational imaging to visualize TCC in a mouse model in 3 dimensions,

as a prototype for similar use in human TCC. Our approach allows for a significantly improved detailed window into the pathogenesis of the tumor, including invasion of the bladder wall and heterogeneities within the tumor. These pathological hallmarks are frequently observed in human-excised tissue. Currently, MRI 3-D reconstruction of the bladder is less common than traditional cystoscopic evaluation despite the fact that it is less invasive than cystoscopy, and important observations, including tumor staging, may be missed. The challenge in translating this technology to humans, where the tumor will be much smaller relative to the entire bladder at the time of imaging, will be improving the specificity for TCC to obtain the strongest signal possible. However, we predict that through additional research, a combination of MRI and fluorescent cystoscopy aided by MSN will make it possible to more accurately assess human TCC, and ultimately, if caught at a sufficiently early stage, improve patient prognosis.

Authors' contributions

All authors contributed equally to this publication. All authors read and approved the final manuscript.

Author details

¹ Department of Biomedical Engineering, University of Iowa, 1402 Seamans Center for the Engineering Arts and Sciences, Iowa City, IA 52242, USA. ² NanoMedTriX, LLC, 2500 Crosspark Road, Suite E119, Coralville, IA 52241-4710, USA. ³ Department of Urology, University of Iowa, Roy J. and Lucille A. Carver College of Medicine, 3204 Medical Education Research Facility, 375 Newton Road, Iowa City, IA 52242, USA. ⁴ Department of Urology, University of Iowa, Roy J. and Lucille A. Carver College of Medicine, 200 Hawkins Dr., Iowa City, IA 52242, USA.

Acknowledgements

The particles manufactured in this manuscript are protected by provisional patent filing serial number 61/645,712, "Multimodal Imaging Methods Using Mesoporous Silica Nanoparticles," filed May 11, 2012. The work is funded by Iowa Economic Development Authority Demonstration Fund #13-DEMO-005, and NSF SBIR Grant #IIP-1345646. The authors would also like to acknowledge Dan Thedens, Associate Research Scientist, Department of Radiology, University of Iowa, for his assistance with MRI scans, and Nathan Black for technical assistance with MSN synthesis and characterization.

Competing interests

JA is founder and sole proprietor of NanoMedTriX, LLC, which prepared the nanoparticles used in this study. All results and claims have been independently verified by other scientists with no financial stake in the company.

Received: 9 December 2015 Accepted: 7 April 2016

Published online: 27 April 2016

References

- Athanasios KA, Niederauer GG, Agrawal CM. Sterilization, toxicity, biocompatibility and clinical applications of polylactic acid/polyglycolic acid copolymers. *Biomaterials*. 1996;17(2):93–102.
- Benezra M, Penate-Medina O, Zanzonico PB, Schaer D, Ow H, Burns A, DeStanchina E, Longo V, Herz E, Iyer S, Wolchok J, Larson SM, Wiesner U, Bradbury MS. Multimodal silica nanoparticles are effective cancer-targeted probes in a model of human melanoma. *J Clin Invest*. 2011;121(7):2768–80. doi:10.1172/JCI45600.
- Bockholt NA, Knudson MJ, Henning JR, Maymi JL, Weady P, Smith GJ, Eisenbraun MD, Fraser JD, O'Donnell MA, Luo Y. Anti-interleukin-10R1 monoclonal antibody enhances bacillus Calmette-Guerin induced T-helper type 1 immune responses and antitumor immunity in a mouse orthotopic model of bladder cancer. *J Urol*. 2012;187(6):2228–35. doi:10.1016/j.juro.2012.01.030.
- Bouchelouche K, Choyke PL. PET/computed tomography in renal, bladder, and testicular cancer. *PET Clin*. 2015;10(3):361–74. doi:10.1016/j.cpet.2015.03.002.
- Brausi M, Oddens J, Sylvester R, Bono A, van de Beek C, van Andel G, Gontero P, Turkeri L, Marreud S, Collette S, Oosterlinck W. Side effects of Bacillus Calmette-Guerin (BCG) in the treatment of intermediate- and high-risk Ta, T1 papillary carcinoma of the bladder: results of the EORTC genito-urinary cancers group randomised phase 3 study comparing one-third dose with full dose and 1 year with 3 years of maintenance BCG. *Eur Urol*. 2014;65(1):69–76. doi:10.1016/j.eururo.2013.07.021.
- Bridot JL, Faure AC, Laurent S, Riviere C, Billotey C, Hiba B, Janier M, Jossierand V, Coll JL, Elst LV, Muller R, Roux S, Perriat P, Tillement O. Hybrid gadolinium oxide nanoparticles: multimodal contrast agents for in vivo imaging. *J Am Chem Soc*. 2007;129(16):5076–84. doi:10.1021/ja068356j.
- Brown LF, Berse B, Jackman RW, Tognazzi K, Manseau EJ, Dvorak HF, Senger DR. Increased expression of vascular permeability factor (vascular endothelial growth factor) and its receptors in kidney and bladder carcinomas. *Am J Pathol*. 1993;143(5):1255–62.
- Bryan RT, Shimwell NJ, Wei W, Devall AJ, Pirrie SJ, James ND, Zeegers MP, Cheng KK, Martin A, Ward DG. Urinary EpCAM in urothelial bladder cancer patients: characterisation and evaluation of biomarker potential. *Br J Cancer*. 2014;110(3):679–85. doi:10.1038/bjc.2013.744.

- Bubenik J, Baresova M, Viklicky V, Jakoubkova J, Sainerova H, Donner J. Established cell line of urinary bladder carcinoma (T24) containing tumour-specific antigen. *Int J Cancer*. 1973;11(3):765–73.
- Chan MH, Lin HM. Preparation and identification of multifunctional mesoporous silica nanoparticles for in vitro and in vivo dual-mode imaging, theranostics, and targeted tracking. *Biomaterials*. 2015;46:149–58. doi:[10.1016/j.biomaterials.2014.12.034](https://doi.org/10.1016/j.biomaterials.2014.12.034).
- Chan E, Patel A, Heston W, Larchian W. Mouse orthotopic models for bladder cancer research. *BJU Int*. 2009;104(9):1286–91. doi:[10.1111/j.1464-410X.2009.08577.x](https://doi.org/10.1111/j.1464-410X.2009.08577.x).
- Chen Y, Chen H, Zeng D, Tian Y, Chen F, Feng J, Shi J. Core/shell structured hollow mesoporous nanocapsules: a potential platform for simultaneous cell imaging and anticancer drug delivery. *ACS Nano*. 2010;4(10):6001–13. doi:[10.1021/nn1015117](https://doi.org/10.1021/nn1015117).
- Cheng L, Montironi R, Davidson DD, Lopez-Beltran A. Staging and reporting of urothelial carcinoma of the urinary bladder. *Mod Pathol*. 2009;22(Suppl 2):S70–95. doi:[10.1038/modpathol.2009.1](https://doi.org/10.1038/modpathol.2009.1).
- Cheng L, Neumann RM, Weaver AL, Chevillat JC, Leibovich BC, Ramnani DM, Scherer BG, Nehra A, Zincke H, Bostwick DG. Grading and staging of bladder carcinoma in transurethral resection specimens. Correlation with 105 matched cystectomy specimens. *Am J Clin Pathol*. 2000;113(2):275–9. doi:[10.1309/94B6-8VFB-MN9J-1NF5](https://doi.org/10.1309/94B6-8VFB-MN9J-1NF5).
- Connolly D, Curran S, Paull B. Polymeric monolithic materials modified with nanoparticles for separation and detection of biomolecules: a review. *Proteomics*. 2012;12(19–20):2904–17. doi:[10.1002/pmic.201200142](https://doi.org/10.1002/pmic.201200142).
- Cozzi PJ, Malhotra S, McAuliffe P, Kooby DA, Federoff HJ, Huryk B, Johnson P, Scardino PT, Heston WD, Fong Y. Intravesical oncolytic viral therapy using attenuated, replication-competent herpes simplex viruses G207 and Nv1020 is effective in the treatment of bladder cancer in an orthotopic syngeneic model. *FASEB J*. 2001;15(7):1306–8.
- Dalbagni G, Vora K, Kaag M, Cronin A, Bochner B, Donat SM, Herr HW. Clinical outcome in a contemporary series of restaged patients with clinical T1 bladder cancer. *Eur Urol*. 2009;56(6):903–10. doi:[10.1016/j.eururo.2009.07.005](https://doi.org/10.1016/j.eururo.2009.07.005).
- Faba OR, Palou J, Breda A, Villavicencio H. High-risk non-muscle-invasive bladder cancer: update for a better identification and treatment. *World J Urol*. 2012;30(6):833–40. doi:[10.1007/s00345-012-0967-1](https://doi.org/10.1007/s00345-012-0967-1).
- Filbeck T, Pichlmeier U, Knuechel R, Wieland WF, Roessler W. Do patients profit from 5-aminolevulinic acid-induced fluorescence diagnosis in transurethral resection of bladder carcinoma? *Urology*. 2002;60(6):1025–8.
- Gakis G, Efstathiou J, Lerner SP, Cookson MS, Keegan KA, Guru KA, Shipley WU, Heidenreich A, Schoenberg MP, Sagalowsky AI, Soloway MS, Stenzl A. International Consultation on Urologic Disease-European Association of Urology Consultation on Bladder Cancer 2012 (2013) ICDU-EAU International Consultation on Bladder Cancer 2012: radical cystectomy and bladder preservation for muscle-invasive urothelial carcinoma of the bladder. *Eur Urol*. 2013;63(1):45–57. doi:[10.1016/j.eururo.2012.08.009](https://doi.org/10.1016/j.eururo.2012.08.009).
- Giri S, Trewyn BG, Stellmaker MP, Lin VS. Stimuli-responsive controlled-release delivery system based on mesoporous silica nanorods capped with magnetic nanoparticles. *Angew Chem Int Ed Engl*. 2005;44(32):5038–44. doi:[10.1002/anie.200501819](https://doi.org/10.1002/anie.200501819).
- Gkritsiotis P, Hatzimouratidis K, Kazantzidis S, Dimitriadis G, Ioannidis E, Katsikas V. Hexaminolevulinic acid-guided transurethral resection of non-muscle-invasive bladder cancer does not reduce the recurrence rates after a 2-year follow-up: a prospective randomized trial. *Int Urol Nephrol*. 2014;46(5):927–33. doi:[10.1007/s11255-013-0603-z](https://doi.org/10.1007/s11255-013-0603-z).
- Gontero P, Banisadr S, Frea B, Brausi M. Metastasis markers in bladder cancer: a review of the literature and clinical considerations. *Eur Urol*. 2004;46(3):296–311. doi:[10.1016/j.eururo.2004.04.001](https://doi.org/10.1016/j.eururo.2004.04.001).
- Grabnar I, Bogataj M, Belic A, Logar V, Karba R, Mrhar A. Kinetic model of drug distribution in the urinary bladder wall following intravesical instillation. *Int J Pharm*. 2006;322(1–2):52–9.
- Grossman HB, Soloway M, Messing E, Katz G, Stein B, Kassabian V, Shen Y. Surveillance for recurrent bladder cancer using a point-of-care proteomic assay. *JAMA*. 2006;295(3):299–305.
- Gruenhagen JA, Lai CY, Radu DR, Lin VS, Yeung ES. Real-time imaging of tunable adenosine 5-triphosphate release from an MCM-41-type mesoporous silica nanosphere-based delivery system. *Appl Spectrosc*. 2005;59(4):424–31.
- GuhaSarkar S, Banerjee R. Intravesical drug delivery: challenges, current status, opportunities and novel strategies. *J Control Release*. 2010;148(2):147–59. doi:[10.1016/j.jconrel.2010.08.031](https://doi.org/10.1016/j.jconrel.2010.08.031).
- Hall MC, Chang SS, Dalbagni G, Pruthi RS, Seigne JD, Skinner EC, Wolf JS Jr, Schellhammer PF. Guideline for the management of nonmuscle invasive bladder cancer (stages Ta, T1, and Tis): 2007 update. *J Urol*. 2007;178(6):2314–30.
- Hermanson GT. *Bioconjugate Techniques*. 2nd ed. Burlington: Elsevier Academic Press; 2008.
- Hoiland-Carlson PF, Poulsen MH, Petersen H, Hess S, Lund L. FDG in urologic malignancies. *PET Clin*. 2014;9(4):457–68. doi:[10.1016/j.cpet.2014.07.003](https://doi.org/10.1016/j.cpet.2014.07.003).
- Hong CW, Rais-Bahrami S, Walton-Diaz A, Shakir N, Su D, George AK, Merino MJ, Turkbey B, Choyke PL, Wood BJ, Pinto PA. Comparison of magnetic resonance imaging and ultrasound (MRI-US) fusion-guided prostate biopsies obtained from axial and sagittal approaches. *BJU Int*. 2015;115(5):772–9. doi:[10.1111/bju.12871](https://doi.org/10.1111/bju.12871).
- Hsiao JK, Tsai CP, Chung TH, Hung Y, Yao M, Liu HM, Mou CY, Yang CS, Chen YC, Huang DM. Mesoporous silica nanoparticles as a delivery system of gadolinium for effective human stem cell tracking. *Small*. 2008;4(9):1445–52. doi:[10.1002/smll.200701316](https://doi.org/10.1002/smll.200701316).
- Huang DM, Hung Y, Ko BS, Hsu SC, Chen WH, Chien CL, Tsai CP, Kuo CT, Kang JC, Yang CS, Mou CY, Chen YC. Highly efficient cellular labeling of mesoporous nanoparticles in human mesenchymal stem cells: implication for stem cell tracking. *FASEB J*. 2005;19(14):2014–6.
- Huang C, Neoh KG, Xu L, Kang ET, Chiong E. Polymeric nanoparticles with encapsulated superparamagnetic iron oxide and conjugated cisplatin for potential bladder cancer therapy. *Biomacromolecules*. 2012;13(8):2513–20. doi:[10.1021/bm300739w](https://doi.org/10.1021/bm300739w).
- Joudi FN, Konety BR. Fluorescence cystoscopy and bladder surveillance. *Curr Opin Urol*. 2004;14(5):265–70.
- Kaufman DS. Challenges in the treatment of bladder cancer. *Ann Oncol*. 2006;17(Suppl 5):v106–12.
- Kaufman DS, Shipley WU, Feldman AS. Bladder cancer. *Lancet*. 2009;374(9685):239–49. doi:[10.1016/S0140-6736\(09\)60491-8](https://doi.org/10.1016/S0140-6736(09)60491-8).
- Kim JC, Steinberg GD. The limits of bacillus Calmette-Guerin for carcinoma in situ of the bladder. *J Urol*. 2001;165(3):745–56.

- Kirchner C, Liedl T, Kudera S, Pellegrino T, Munoz Javier A, Gaub HE, Stolze S, Fertig N, Parak WJ. Cytotoxicity of colloidal CdSe and CdSe/ZnS nanoparticles. *Nano Lett.* 2005;5(2):331–8. doi:10.1021/nl047996m.
- Knowles LM, Zewe J, Malik G, Parwani AV, Gingrich JR, Pilch J. CLT1 targets bladder cancer through integrin alpha5beta1 and CLIC3. *Mol Cancer Res.* 2013;11(2):194–203. doi:10.1158/1541-7786.MCR-12-0300.
- Kowalski M, Entwistle J, Cizeau J, Niforos D, Loewen S, Chapman W, MacDonald GC. A phase I study of an intravesically administered immunotoxin targeting EpCAM for the treatment of nonmuscle-invasive bladder cancer in BCGrefractory and BCG-intolerant patients. *Drug Des Devel Ther.* 2010;4:313–20. doi:10.2147/DDDT.S14071.
- Kriegmair M, Baumgartner R, Riesenberger R, Jocham D, Sassy T, Stocker S, Lumper W, Unsold E, Hofstetter A. Photodynamic diagnosis following topical application of delta-aminolevulinic acid in a rat bladder tumor model. *Investig Urol (Berl).* 1994;5:85–7.
- Lamm DL, Blumenstein BA, Crissman JD, Montie JE, Gottesman JE, Lowe BA, Sarosdy MF, Bohl RD, Grossman HB, Beck TM, Leimert JT, Crawford ED. Maintenance bacillus Calmette-Guerin immunotherapy for recurrent TA, T1 and carcinoma in situ transitional cell carcinoma of the bladder: a randomized Southwest Oncology Group Study. *J Urol.* 2000;163(4):1124–9.
- Larsen EK, Nielsen T, Wittenborn T, Birkedal H, Vorup-Jensen T, Jakobsen MH, Ostergaard L, Horsman MR, Besenbacher F, Howard KA, Kjems J. Size-dependent accumulation of PEGylated silane-coated magnetic iron oxide nanoparticles in murine tumors. *ACS Nano.* 2009;3(7):1947–51. doi:10.1021/nn900330m.
- Liu JJ, Droller MJ, Liao JC. New optical imaging technologies for bladder cancer: considerations and perspectives. *J Urol.* 2012;188(2):361–8. doi:10.1016/j.juro.2012.03.127.
- Liu T, Xing R, Zhou YF, Zhang J, Su YY, Zhang KQ, He Y, Sima YH, Xu SQ. Hematopoiesis toxicity induced by CdTe quantum dots determined in an invertebrate model organism. *Biomaterials.* 2014;35(9):2942–51. doi:10.1016/j.biomaterials.2013.12.007.
- Lu J, Choi E, Tamanoi F, Zink JI. Light-activated nanopump-controlled drug release in cancer cells. *Small.* 2008;4(4):421–6. doi:10.1002/smll.200700903.
- Lu J, Liong M, Li Z, Zink JI, Tamanoi F. Biocompatibility, biodistribution, and drug-delivery efficiency of mesoporous silica nanoparticles for cancer therapy in animals. *Small.* 2010;6(16):1794–805. doi:10.1002/smll.201000538.
- Luo Y, Chen X, O'Donnell MA. Use of prostate specific antigen to measure bladder tumor growth in a mouse orthotopic model. *J Urol.* 2004;172(6 Pt 1):2414–20.
- Luo T, Huang P, Gao G, Shen G, Fu S, Cui D, Zhou C, Ren Q. Mesoporous silica-coated gold nanorods with embedded indocyanine green for dual mode X-ray CT and NIR fluorescence imaging. *Opt Express.* 2011;19(18):17030–9. doi:10.1364/OE.19.017030.
- Martocchia C, Zellweger M, Lovisa B, Jichlinski P, van den Bergh H, Wagnieres G. Optical spectroscopy of the bladder washout fluid to optimize fluorescence cystoscopy with Hexvix(R). *J Biomed Opt.* 2014;19(9):97002. doi:10.1117/1.JBO.19.9.097002.
- Mitra AP, Jorda M, Cote RJ. Pathological possibilities and pitfalls in detecting aggressive bladder cancer. *Curr Opin Urol.* 2012;22(5):397–404. doi:10.1097/MOU.0b013e328356ade6.
- Nakamura T, Fukiage M, Higuchi M, Nakaya A, Yano I, Miyazaki J, Nishiyama H, Akaza H, Ito T, Hosokawa H, Nakayama T, Harashina H. Nanoparticulation of BCG-CWS for application to bladder cancer therapy. *J Control Release.* 2014;176:44–53. doi:10.1016/j.jconrel.2013.12.027.
- Nargund VH, Tanabalan CK, Kabir MN. Management of non-muscle-invasive (superficial) bladder cancer. *Semin Oncol.* 2012;39(5):559–72. doi:10.1053/j.seminoncol.2012.08.001.
- Nemoto R, Mori H, Iwata K, Kato T, Harada M. A model of malignant urinary bladder tumor in rabbits. *Tohoku J Exp Med.* 1981;134(3):257–63.
- Newton MR, Askeland EJ, Andresen ED, Chehval VA, Wang X, Askeland RW, O'Donnell MA, Luo Y. Anti-interleukin-10R1 monoclonal antibody in combination with bacillus Calmette-Guerin is protective against bladder cancer metastasis in a murine orthotopic tumour model and demonstrates systemic specific anti-tumour immunity. *Clin Exp Immunol.* 2014;177(1):261–8. doi:10.1111/cei.12315.
- Nyland TG, Wallack ST, Wisner ER. Needle-tract implantation following us-guided fine-needle aspiration biopsy of transitional cell carcinoma of the bladder, urethra, and prostate. *Vet Radiol Ultrasound.* 2002;43(1):50–3.
- Ochiai T, Sato H, Hayashi R, Asano T, Sato H, Yamamura Y. Postoperative adjuvant immunotherapy of gastric cancer with BCG-cell wall skeleton. 3- to 6-year follow up of a randomized clinical trial. *Cancer Immunol Immunother.* 1983;14(3):167–71.
- Parker N, Turk MJ, Westrick E, Lewis JD, Low PS, Leamon CP. Folate receptor expression in carcinomas and normal tissues determined by a quantitative radioligand binding assay. *Anal Biochem.* 2005;338(2):284–93.
- Raza SA, Jhaveri KS. MR imaging of urinary bladder carcinoma and beyond. *Radiol Clin North Am.* 2012;50(6):1085–110. doi:10.1016/j.rcl.2012.08.011.
- Salvado O, Hillenbrand CM, Wilson DL. Partial volume reduction by interpolation with reverse diffusion. *Int J Biomed Imaging.* 2006b;2006:92092. doi:10.1155/IJBI/2006/92092.
- Salvado O, Hillenbrand C, Zhang S, Wilson DL. Method to correct intensity inhomogeneity in MR images for atherosclerosis characterization. *IEEE Trans Med Imaging.* 2006a;25(5):539–52. doi:10.1109/TMI.2006.871418.
- Seideman C, Canter D, Kim P, Cordon B, Weizer A, Oliva I, Rao J, Inman BA, Posch M, Herr H, Lotan Y. Multicenter evaluation of the role of UroVysion FISH assay in surveillance of patients with bladder cancer: does FISH positivity anticipate recurrence? *World J Urol.* 2015;33(9):1309–13. doi:10.1007/s00345-014-1452-9.
- Selvan ST, Tan TT, Yi DK, Jana NR. Functional and multifunctional nanoparticles for bioimaging and biosensing. *Langmuir.* 2010;26(14):11631–41. doi:10.1021/la903512m.
- Semete B, Booyesen L, Lemmer Y, Kalombo L, Katata L, Verschoor J, Swai HS. In vivo evaluation of the biodistribution and safety of PLGA nanoparticles as drug delivery systems. *Nanomedicine.* 2010;6(5):662–71. doi:10.1016/j.nano.2010.02.002.
- Siegel RL, Miller KD, Jemal A. Cancer statistics 2015. *CA Cancer J Clin.* 2015;65(1):5–29. doi:10.3322/caac.21254.
- Slowing I, Trewny BG, Lin VS. Effect of surface functionalization of MCM-41-type mesoporous silica nanoparticles on the endocytosis by human cancer cells. *J Am Chem Soc.* 2006;128(46):14792–3. doi:10.1021/ja0645943.

- Slowing II, Trewyn BG, Lin VS. Mesoporous silica nanoparticles for intracellular delivery of membrane-impermeable proteins. *J Am Chem Soc.* 2007;129(28):8845–9. doi:[10.1021/ja0719780](https://doi.org/10.1021/ja0719780).
- Soloway MS, deKernion JB, Rose D, Persky L. Effect of chemotherapeutic agents on bladder cancer: a new animal model. *Surg Forum.* 1973;24:542–4.
- Summerhayes IC, Franks LM. Effects of donor age on neoplastic transformation of adult mouse bladder epithelium in vitro. *J Natl Cancer Inst.* 1979;62(4):1017–23.
- Tagaya M, Ikoma T, Xu Z, Tanaka J. Synthesis of luminescent nanoporous silica spheres functionalized with folic acid for targeting to cancer cells. *Inorg Chem.* 2014;53(13):6817–27. doi:[10.1021/ic500609g](https://doi.org/10.1021/ic500609g).
- Vergara-Lluri ME, Hu E, Rao JY, Levin M, Apple SK, Moatamed NA. Comparative evaluation of ProEx C and ImmunoCyt/uCyt assays in atypical urine cytology. *Arch Pathol Lab Med.* 2014;138(9):1215–22. doi:[10.5858/arpa.2013-0433-OA](https://doi.org/10.5858/arpa.2013-0433-OA).
- Wang Y, Zhao Q, Han N, Bai L, Li J, Liu J, Che E, Hu L, Zhang Q, Jiang T, Wang S. Mesoporous silica nanoparticles in drug delivery and biomedical applications. *Nanomedicine.* 2015;11(2):313–27. doi:[10.1016/j.nano.2014.09.014](https://doi.org/10.1016/j.nano.2014.09.014).
- Zaak D, Karl A, Knuchel R, Stepp H, Hartmann A, Reich O, Bachmann A, Siebels M, Popken G, Stief C. Diagnosis of urothelial carcinoma of the bladder using fluorescence endoscopy. *BJU Int.* 2005;96(2):217–22.
- Zhang N, Li D, Shao J, Wang X. Animal models for bladder cancer: the model establishment and evaluation (review). *Oncol Lett.* 2015;9(4):1515–9. doi:[10.3892/ol.2015.2888](https://doi.org/10.3892/ol.2015.2888).

Submit your manuscript to a SpringerOpen[®] journal and benefit from:

- ▶ Convenient online submission
- ▶ Rigorous peer review
- ▶ Immediate publication on acceptance
- ▶ Open access: articles freely available online
- ▶ High visibility within the field
- ▶ Retaining the copyright to your article

Submit your next manuscript at ▶ springeropen.com
